THE JOURNAL OF PHYSICAL CHEMISTRY B

ARTICLE

pubs.acs.org/JPCB

Thermal Hysteresis in the Backbone and Side-Chain Dynamics of the Elastin Mimetic Peptide $[VPGVG]_3$ Revealed by ^2H NMR

Xiang Ma, Cheng Sun, Jiaxin Huang, and Gregory S. Boutis*

Department of Physics, Brooklyn College of the City University of New York, 2900 Bedford Avenue, Brooklyn, New York 11210, United States

ABSTRACT: We report on experimental measurements of the backbone and side-chain dynamics of the elastin mimetic peptide $[VPGVG]_3$ by ^2H NMR echo spectroscopy and 2D T_1-T_2 correlation relaxometry. The T_1 and T_2 relaxation times of the Gly α-deuterons and Val α-, β-, and γ-deuterons of a hydrated sample reveal a thermal hysteresis when the temperature is raised from −10 to 45 °C and then subsequently cooled back to −10 °C. In addition, near 30 °C we observe a reduction in the slope of the $T_1(T)$ and $T_2(T)$ heating curves, indicating a structural change that appears to be correlated well to the known inverse temperature transition of this peptide. The thermal dependence of the correlation times of the Gly α-deuterons are well fit by an Arrhenius Law, from which we measured $E_{act} = (20.0 \pm 3.1)$ kJ/mol when the sample is heated and $E_{act} = (10.9 \pm 2.8)$ kJ/mol when cooled. Molecular dynamics simulations support the notion that the measured activation energy is determined largely by the extent of localized water, which is observed to decrease with increasing temperature from approximately 25 to 42 °C.

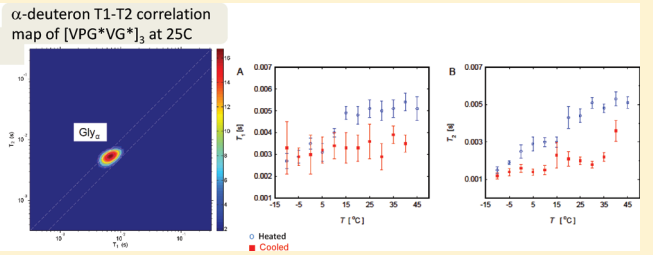

INTRODUCTION

Elastin is an intriguing protein that provides vertebrate tissues with their elastomeric properties.[1−4] The elasticity of this remarkable protein is known to hinge on a complex interaction with the solvent; elastin is only elastic when hydrated.[5] For example, experimental measurements of the Young's modulus demonstrated a dependence of the stress−strain relationship on solvent polarity.[6−8] A well-known characteristic of elastin is that it undergoes an inverse temperature transition at approximately 20−40 °C, a process that results in a reduction in the protein radius of gyration, expulsion of water, and formation of a complex network of hydrogen bonds.[1,9] It has been experimentally demonstrated that the repeating elastin motif $[VPGVG]_n$ undergoes an inverse temperature transition and lends itself as a simplified model of the more complex protein.[9−12] Simulation studies have demonstrated that the physical signatures of the inverse temperature transition of $[VPGVG]_{18}$ include a decrease in the radius of gyration of the α-carbons, number of localized water molecules, and number of peptide−water hydrogen bonds as the temperature is increased from approximately 20 to 40 °C.[13] In addition, as the temperature is increased over this range, there is an observed increase in the number of peptide side-chain contacts and number of peptide−peptide hydrogen bonds. A variety of structural studies of elastin have been performed that have demonstrated the presence of twisted-rope-like organization as well as the presence of α-helical and β-turn conformations.[1,14−17] The type II β-turn was observed in simulations of a $[VPGVG]_{18}$ peptide[13] and in experimental studies of $[(VPGVG)_4(VPGKG)]_{39}$[18] and $[VPGVG]_3$[19] using nuclear magnetic resonance (NMR). Moreover, the dynamical properties of short elastin mimetic peptides appeared to hinge on a complex interaction with the solvent.[20] In our work the backbone and side-chain dynamics of the elastin mimetic peptide $[VPGVG]_3$ are studied using ^2H quadrupolar echo spectroscopy[21] and 2D T_1-T_2 correlation NMR.[22] The experimental data reveal a thermal hysteresis of the T_1 and T_2 relaxation times as the sample is heated from −10 to 45 °C and then subsequently cooled. This observation appears to be correlated to that observed by other experimental schemes.[23] In addition, the data show a reduction in the slope of the $T_1(T)$ and $T_2(T)$ heating curves near 30 °C, indicating a structural change that appears to be in good agreement with the notion of an inverse temperature transition.

Quadrupolar echo spectroscopy is a well-known experimental technique that allows for studying the structure and dynamics of selectively deuterium-labeled sites of a broad range of materials.[21] The NMR line shape in this experimental scheme is determined largely by the quadrupolar Hamiltonian. The coupling between the nuclear quadrupolar moment and electric field gradient is affected by the orientation and motion of the labeled segment. A deuterium line shape can be analyzed in terms of restricted anisotropic motion by comparing the experimental data with a simulated spectrum.[24,25] Quadrupolar echo experiments probe the large dynamic range from 10^{-7} to 10^{-3} s. The molecular motion of side chains, for instance, has been extensively studied by deuterium NMR in a broad range of systems, providing detailed information relating to the structure and dynamics (see refs 26−33, for example). The 2D T_1-T_2 correlation NMR technique is a powerful tool to study the dynamics of multisite systems.[22,34,35] By implementing a 2D inverse Laplace transform (ILT), the T_1 and T_2 relaxation times of a site are

Received: September 16, 2011
Revised: November 30, 2011
Published: December 02, 2011

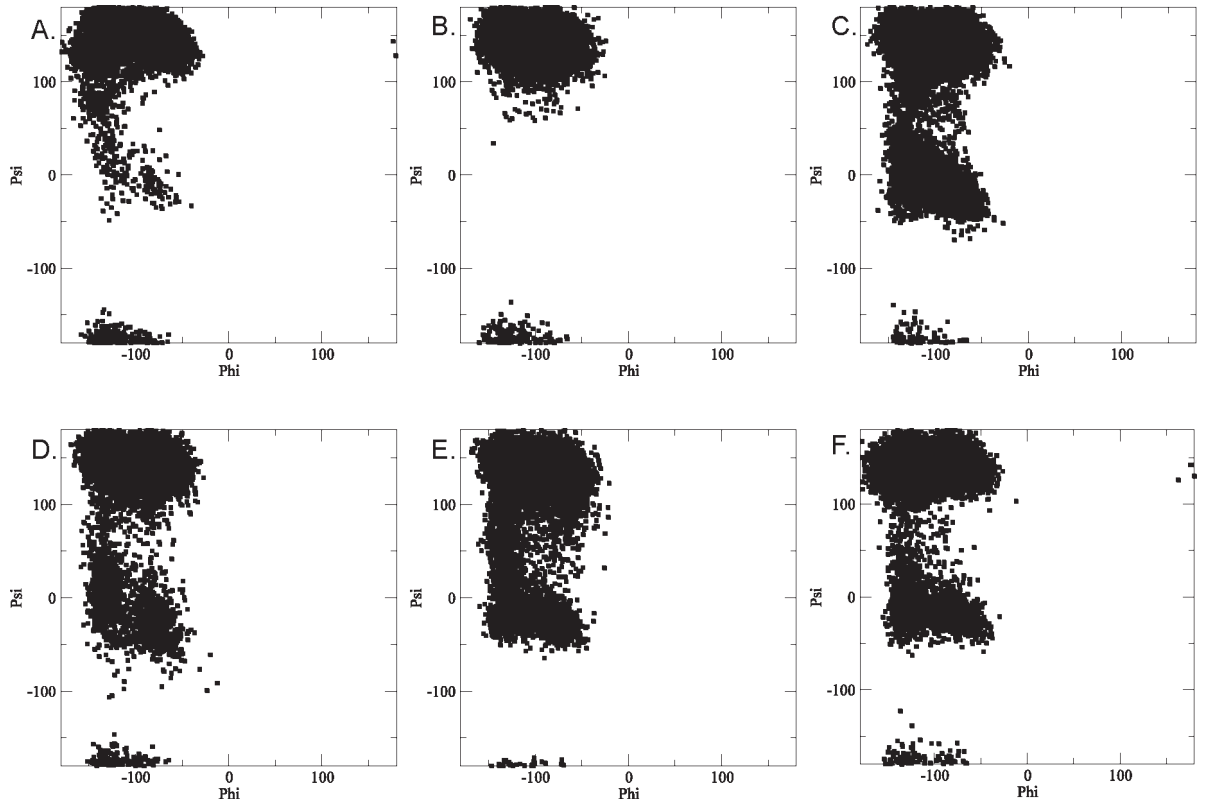

Figure 1. Valine Ramachandran maps of water-solvated $[VPGVG]_3$ peptide derived from MD simulation at (A) 10, (B) 20, (C) 25, (D) 30, (E) 35, and (F) 42 °C.

Table 1. MD-Derived Simulation Results for $[VPGVG]_3$[a]

temp (°C)	R_g[b] (nm)	side-chain contacts[c]	no. of water molecules[d]	peptide−peptide hydrogen bonds[e]	peptide−water hydrogen bonds[e]
5	1.26 ± 0.06	143 ± 3	369 ± 26	0.03 ± 0.16	31.6 ± 2.7
10	1.98 ± 0.08	153 ± 5	365 ± 27	0.10 ± 0.31	30.2 ± 2.7
20	1.06 ± 0.05	143 ± 3	367 ± 28	0.02 ± 0.14	31.0 ± 2.9
25	1.01 ± 0.07	152 ± 7	342 ± 26	0.10 ± 0.31	29.7 ± 2.8
30	1.13 ± 0.08	142 ± 3	355 ± 26	0.14 ± 0.40	30.0 ± 3.0
35	0.79 ± 0.04	156 ± 6	324 ± 26	0.61 ± 0.65	27.5 ± 2.9
42	0.83 ± 0.07	158 ± 8	316 ± 28	0.35 ± 0.60	28.1 ± 2.9
50	0.63 ± 0.02	180 ± 11	289 ± 31	1.47 ± 1.01	24.0 ± 3.0

[a] The values shown in the table were determined by performing computations over all residues of the peptide. All values shown in the table represent the average and standard deviation over the last 1 ns of the 4 ns MD simulation at the specified temperature. [b] The radius of gyration (R_g) was determined by computing the position of all C_α carbons. [c] Side-chain contacts were counted when two neighboring aliphatic carbon atoms from neighboring residues were within 0.54 nm of each other. [d] Number of water molecules were counted when a water molecule was within 0.3 nm of any peptide atoms. [e] Hydrogen bonds were counted when the donor−acceptor cutoff distance of 0.35 nm and the hydrogen-donor−acceptor angle of 30° was satisfied.

correlated and manifested into a peak in a 2D map. The T_1/T_2 ratio obtained from the 2D T_1-T_2 correlation map may be used to study the mechanism of relaxation in porous media.[36,37] This method has recently been employed to study the porous properties of water-saturated sedimentary rocks,[38] in potato tissue,[39] in cement pastes,[40] and in the study of exchange of water in hydrated elastin.[41]

MATERIALS AND METHODS

Two deuterium-labeled $[VPGVG]_3$ peptide samples were synthesized by California Peptide and New England Peptide using methods discussed in ref 1. On one sample, denoted $[VPG^*VG^*]_3$, all Gly α-protons were substituted with ^2H. In the second sample, denoted $[VPGV^*G]_3$, the Val α-, β-, and γ-protons on Val4, Val9, and Val14 were substituted with ^2H. Both peptides were terminated by the acetyl and amine group at the C- and N-termini, respectively. The measured purity of the samples was >99.0%, and the mass was within 0.1% of the expected molecular weight. Deuterium NMR experiments were performed on lyophilized and H_2O-hydrated peptides using a 200 MHz Tecmag Apollo NMR system and a home-built NMR probe. A two-pulse quadrupolar echo pulse sequence was employed to study the ^2H NMR spectrum of the lyophilized peptides with a

phase cycling scheme that suppresses artifacts due to short echo times.[42] Quadrupolar echo spectra were simulated with WEBLAB.[24] The $\pi/2$ radio frequency pulse width in the quadrupolar echo experiment was 2.2 μs, the interpulse spacing was set to 35 μs, and 26 640 scans were accumulated with a recycle delay of 3s. For the water-hydrated peptides, a ^{2}H 2D T_1-T_2 NMR experiment was implemented and the T_1 and T_2 NMR relaxation times were obtained by a 2D ILT of the data.[34] In these experiments, the $\pi/2$ pulse width was 15.9 μs, the interpulse echo time was 180 μs, and 15 points in the T_1 dimension were acquired with 624 scans and a recycle delay of 4s. All of our lyophilized samples were sealed in a 1.7 mm OD capillary tube with a sample size of approximately 5.0 mm^3. Samples were dissolved in water and placed in a capillary tube at a concentration of approximately 0.1 g/mL. Molecular dynamics (MD) simulations were performed on the $[VPGVG]_3$ peptide using the OPLS-AA/L force field model[43] and a Berendsen thermostat[44] in GROMACS.[45] In the MD simulations, the peptides were terminated by the amine ($-NH_2$) and carboxyl ($-COOH$) groups at the N- and C-termini, respectively, and placed in a cubic box solvated with water using the SPC216 water model.[46] At all temperatures the starting peptide structures were linear chains. We performed a short simulation restraining the peptide position and equilibrated the pressure for 10 ps before executing the full simulations. Full simulations were performed for a duration of 4 ns at temperatures ranging from 5 to 50 °C. The dynamical properties of the peptide at all temperatures were determined by averaging over the last 1 ns of the simulation results (i.e., from 3 to 4 ns). Structural equilibrium was verified by observing that the root-mean-square displacement of C_α reached an equilibrated value after 2 ns of simulation.

RESULTS AND DISCUSSION

MD Simulations of $[VPGVG]_3$. The Ramachadran maps of the valine residues are shown in Figure 1, and various MD-derived thermal characteristics of the peptide are tabulated in Table 1. It is clear from Figure 1 that the α-helical structure becomes more prominent above 25 °C than that at lower temperatures. The α-helical structure has also been observed in MD simulations of $[VPGVG]_{18}$[13] and in the oligopeptide GVG(VPGVG).[47] Referring to Table 1, the simulations reveal a decrease in the radius of gyration as well as an increase in the number of side-chain contacts and number of peptide−peptide hydrogen bonds between 20 and 42 °C. In addition, the simulations reveal a decrease in number of water molecules within 0.35 nm of the peptide and number of peptide−water hydrogen bonds between 20 and 42 °C, indicating that water molecules are expelled as the temperature is raised. Our 4 ns simulation findings of the $[VPGVG]_3$ peptide, tabulated in Table 1, appear to be similar to that observed in short 9 ns simulations of $[VPGVG]_{18}$.[13] Figure 1 also highlights the presence of a type II β-turn at all temperatures studied. Observation of a type II β-turn has also been made in simulation studies of $[VPGVG]_{18}$ at 10 and 42 °C[13] and has been experimentally observed in a $[(VPGVG)_4(VPGKG)]_{39}$ peptide by NMR chemical shift analysis.[18]

NMR Studies of Lyophilized $[VPG^*VG^*]_3$ and $[VPGV^*G]_3$. Using the quadrupolar echo pulse sequence, ^{2}H NMR spectra of lyophilized $[VPG^*VG^*]_3$ were obtained at various temperatures and are shown in Figure 2A−E. In addition, a similar experiment was also performed on the water-hydrated $[VPG^*VG^*]_3$ peptide at −30 °C, and the result of this experiment is shown in Figure 2F. In the experiment on the water-hydrated peptide, no pake pattern was observed above −30 °C. To be clear, above −30 °C the broad pake pattern shown in Figure 2E on the water-hydrated sample was not observed but a narrow Lorentzian was measured (with a line width of $1/\pi T_2$) as discussed in the next section. This finding may suggest that the motion of the Gly α-deuterons at −30 °C is quenched due to freezing of localized water.

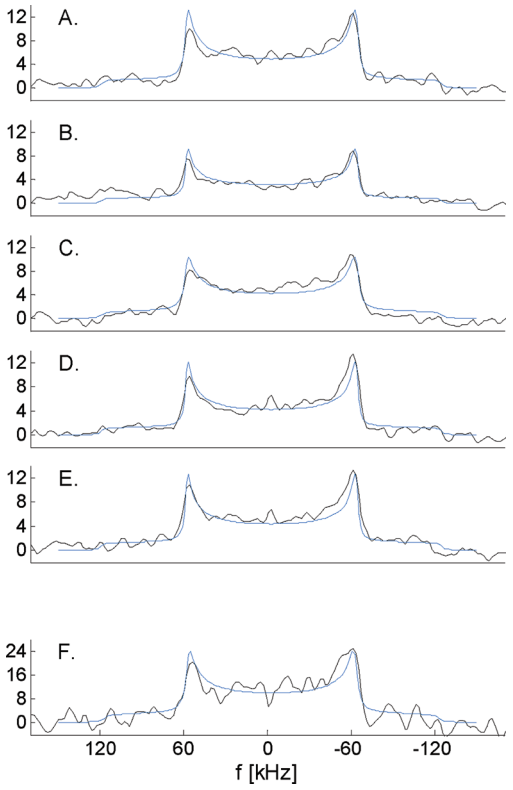

Figure 2. ^{2}H quadrupolar echo NMR spectra of the (A−E) lyophilized $[VPG^*VG^*]_3$ peptide and (F) H_2O-hydrated $[VPG^*VG^*]_3$ peptide: (A) 37, (B) 25, (C) 10, (D) −5, and (E) −20 °C. The spectra shown in F were acquired at −30 °C, where it is believed that localized water near the Gly α-deuterons is frozen, as described in the text. Gaussian broadening of 3 kHz was applied to both simulation and experimental data. Experimental data are indicated by black lines, and simulation results are shown by blue lines.

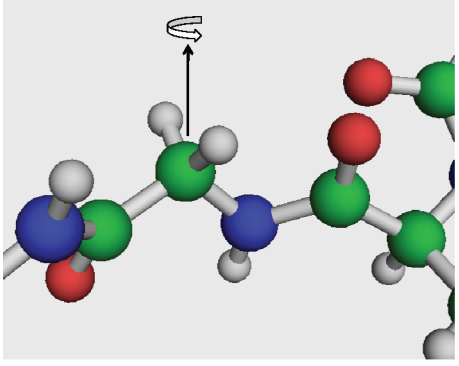

Figure 3. Sketch of the molecular structure of glycine. In the Figure, the arrow defines the axis of rotation assumed in the model described in the text for producing the simulated spectra shown in Figure 2.

dx.doi.org/10.1021/jp208966k | J. Phys. Chem. B 2012, 116, 555–564

Table 2. Parameters Used for Simulating the ^{2}H NMR Quadrupolar Echo Line Shape of the Lyophilized $[VPG^*VG^*]_3$ Spectra Shown in Figure 2[a]

temp (°C)	$\omega_{rot}/2\pi$ (kHz)	$\omega_q/2\pi$ (kHz)
37	3	122
25	3	122
10	3	122
−5	3	122
−20	3	122
−30 (hydrated)	3	120

[a] A two-site jump model was assumed about the axis shown in Figure 3 of the Gly α-deuterons with $\theta = 55.7°$ and $\phi = 180°$, as described in the text.

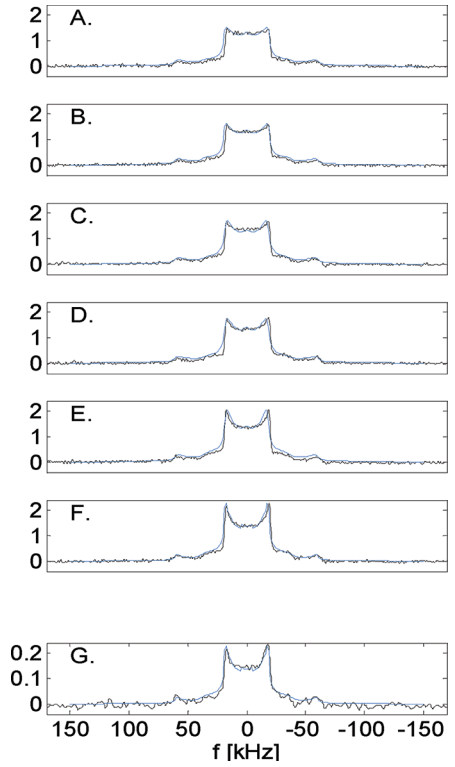

Figure 4. ^{2}H quadrupolar echo NMR spectra of the (A−F) lyophilized $[VPGV^*G]_3$ peptide and (G) H_2O-hydrated $[VPGV^*G]_3$ peptide: (A) 45, (B) 35, (C) 25, (D) 10, (E) −5, and (F) −20 °C. Experimental data shown in G was acquired at −20 °C, where it is believed that the localized water near all the valine deuterons is frozen. Gaussian broadening of 3kHz was applied to both simulation and experimental data. Experimental data are indicated by black lines, and simulation results are shown by blue lines.

The experimental line shapes shown in Figure 2 were simulated in WEBLAB with a model involving two-site jumps of the Gly α-deuterons about the axis indicated by an arrow in Figure 3 with $\theta = 55.7°$ and $\phi = 180°$. In the model, θ is defined by the arrow shown in Figure 3 to the carbon-deuteron bond, and ϕ is defined by the relative phase between the two deuterons. All other motions were assumed very slow and therefore ignored. The simulated spectra are also shown in Figure 2, and the best-fit parameters for the jump rate, ω_{rot}, are provided in Table 2. At all temperatures the quadrupolar asymmetry parameter $\eta = 0$ was assumed in the simulations. The temperature dependence of the quadrupolar frequency, $\omega_q/2\pi$, determined by the simulation is also tabulated in Table 2 and appears to be invariant with temperature. Together the two observations on the lyophilized and water-hydrated sample at −30 °C reveal that the dynamics of the Gly α-deuterons depend heavily on the extent of hydration as well as the mobility of the solvent. An analogous observation was made in the ^{13}C NMR spectra of bovine nuchal ligament elastin.[48] Specifically, the study showed that the mobility of the aliphatic carbons depends dramatically on the extent of hydration, and when the sample was frozen at −20 °C no changes in the spectra were observed over a broad range of hydration levels. Evidence of hydration-dependent dynamics of an elastin mimetic peptide Poly(Lys-25), $[VPGVG_4VPGKG]_{39}$, has also been revealed by ^{13}C NMR.[20] Below 20% hydration the backbone motion of this mimetic peptide was observed to increase slightly, whereas when the peptide was hydrated above 30% both the side chains and the backbone were observed to undergo large amplitude fluctuations.

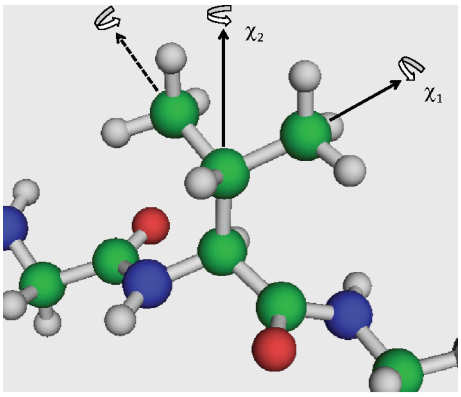

Figure 5. Sketch of the molecular structure of valine. Motion about χ_1 is assumed to be fast (>1 MHz). As described in the text, a superposition of two motions for the Val γ- and β-deuterons is assumed to take place about the $C_\alpha-C_\beta$ axis.

^{2}H NMR quadrupolar echo spectroscopy was also performed on the lyophilized $[VPGV^*G]_3$ peptide, and the spectra are shown in Figure 4A−F. Figure 4G highlights results from the water-hydrated $[VPGV^*G]_3$ peptide at −20 °C. In the experiment on the water-hydrated peptide, no pake pattern was observed above −20 °C and we believe that this observation may be correlated to the freezing of localized water near the Val deuterons, as in the case of the Gly deuterons. One possible reason that the motion of the Val deuterons in the hydrated sample appears to be hindered at −20 °C rather than −30 °C (which was observed in the case of the Gly α-deuterons) may be due to the steric hindrance of the Val side chain. In simulating the line shapes, a superposition of two spectra involving fast and slow motion about the $C_\alpha-C_\beta$ axis (labeled χ_2 in Figure 5) was assumed undergoing three-site jumps with $\theta = 70.6°$ and $\phi = (0°, 120°, 240°)$. The angle θ is defined by the angle between the axes labeled χ_2 and χ_1 in Figure 5 and ϕ is defined by the relative phase of the Val C_γ and C_β sites. Decomposition of the line shape simulated at 45 °C is shown in Figure 6 as an example. At all temperatures the Val α-deuterons were assumed static, and the quadrupolar asymmetry parameter $\eta = 0$ was assumed for all deuterons. The methyl groups were assumed to undergo fast motion with a rotation frequency > 1 MHz about the respective

dx.doi.org/10.1021/jp208966k | J. Phys. Chem. B 2012, 116, 555–564

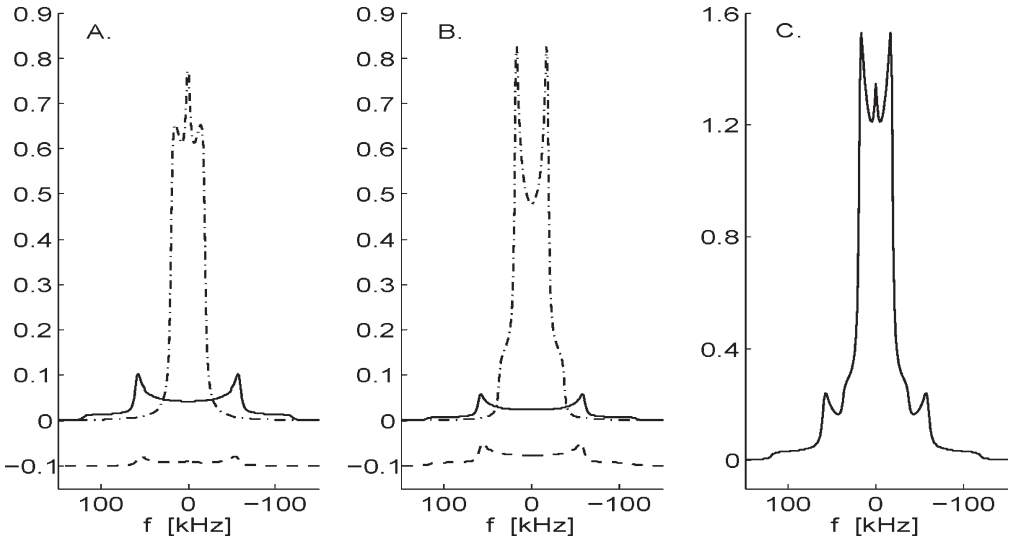

Figure 6. Decomposition of the simulated ^{2}H NMR spectrum of the lyophilized $[VPGV^*G]_3$ peptide at 45 °C: (A) spectra of the fast motion about the $C_\alpha-C_\beta$ axis of valine, (B) slow motion about the $C_\alpha-C_\beta$ axis of valine, and (C) overall spectrum. (A and B) Dot-dashed lines are Val γ-deuterons, solid lines are Val α-deuterons, and dashed lines are Val β-deuterons. Dashed lines are offset by −0.1 for clarity.

Table 3. Parameters Used for Simulating the ^{2}H NMR Quadrupolar Echo Line Shape of the Lyophilized $[VPGV^*G]_3$ Spectra Shown in Figure 4[a]

temp (°C)	slow $\omega_{rot}/2\pi$ (kHz)	fast $\omega_{rot}/2\pi$ (kHz)	Val γ-deuterons $\omega_q/2\pi$ (kHz)	Val α- and β-deuterons $\omega_q/2\pi$ (kHz)	ratio of fast to slow motion
45	3−4	100	38	117	1.8
35	3−4	100	38	117	1.4
25	3−4	30	38	117	0.8
10	3−4	30	38	117	0.8
−5	3−4	30	38	117	0.1
−20	3−4	30	38	117	0.1
−20 (hydrated)	3−4	30	38	117	0.1

[a] A three-site jump model was assumed about the Val $C_\alpha-C_\beta$ axis shown in Figure 5 with $\theta = 70.6°$ and $\phi = (0°, 120°, 240°)$. In the model, methyl rotors were assumed to undergo fast motion (with a rotational frequency > 1 MHz) about the respective $C_\beta-C_\gamma$ axis labeled χ_1 in Figure 5. A superposition of the fast and slow motion of the Val γ- and β-deuterons about the $C_\alpha-C_\beta$ axis was assumed with rotational frequencies indicated by the second and third columns, respectively. The contribution of the fast and slow motion to the total signal is indicated by the last column. As described in the text, the Val α-deuterons were assumed static at all temperatures.

$C_\beta-C_\gamma$ axis (labeled χ_1 in Figure 5). The best-fit parameters for the jump rate of the motions about the $C_\alpha-C_\beta$ axis, ω_{rot}, are listed in Table 3, and the simulated spectra are shown in Figure 4. In simulating the powder line shapes we found a reasonable fit was achieved by assuming a quadrupolar frequency of 117 kHz for the Val α- and β-deuterons and an effective quadrupolar frequency of 38 kHz for the Val γ-deuterons (the effective quadrupolar frequency results from the fast motion of the methyl group about the $C_\beta-C_\gamma$ axis). Referring to Table 3, the slow motion of the Val γ- and β-deuterons about the $C_\alpha-C_\beta$ axis is observed to be independent of the temperature studied and similar to the thermal behavior observed in the Gly α-deuterons of the lyophilized $[VPG^*VG^*]_3$ peptide. However the Val γ- and β-deuterons undergoing fast motion about the $C_\alpha-C_\beta$ axis exhibit a temperature dependence; specifically, a 3-fold increase in mobility is observed above 25 °C. In addition, Table 3 highlights the ratio of the contribution of the fast to slow motion to the total signal. It is observed that this ratio increases with increasing temperature, which may be attributed to side-chain mobility. The requirement of two motions in the line shape fitting may be due to nonuniform packing or dynamical heterogeneity of the three valine residues (i.e., Val4, Val9, and Val14) in the 15-residue peptide. The structural heterogeneity of the valine residues in hydrated $[VPGVG]_3$ is observed in our MD results, highlighted in Figure 1, as well as in simulations of hydrated $[VPGVG]_{18}$.[13] Specifically, one observes the presence of both a α-helix and type II β-turns. In addition, a structural heterogeneity of the valine residues was experimentally observed via solid state NMR in hydrated $[LGGVG]_6$, another repeating motif of elastin.[49]

NMR Studies of Hydrated $[VPG^*VG^*]_3$ and $[VPGV^*G]_3$. The T_1 and T_2 NMR relaxation times of the Gly α-deuterons in the water-hydrated $[VPG^*VG^*]_3$ peptide were measured via the ^{2}H 2D T_1-T_2 correlation NMR technique. The resulting 2D map at 30 °C is shown in Figure 7A as an example. One peak that correlates the T_1 and T_2 relaxation times is observed in Figure 7A, and similar features were revealed for all temperatures studied. The observation of a single peak indicates that all the Gly α-deuterons of the hydrated sample have similar T_1 and T_2 values and therefore have indistinguishable dynamics. Figure 8 highlights the Gly α-deuteron T_1 and T_2 relaxation times as a function

dx.doi.org/10.1021/jp208966k | J. Phys. Chem. B 2012, 116, 555–564

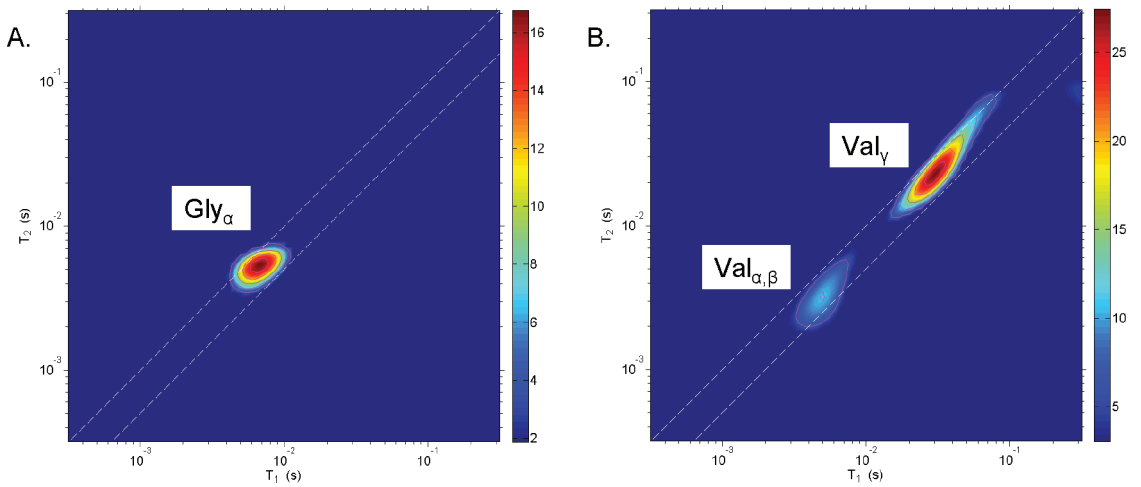

Figure 7. 2D ILT maps of the T_1-T_2 correlation NMR experiments on (A) H_2O-hydrated $[VPG^*VG^*]_3$ peptide at 30 °C and (B) H_2O-hydrated $[VPGV^*G]_3$ peptide at 30 °C. One peak (labeled Gly$_\alpha$) is observed in A, and two peaks (labeled Val$_\gamma$ and Val$_{\alpha,\beta}$) are observed in B. The ratio of the two peaks, corresponding to the Val$_{\alpha,\beta}$ and Val$_\gamma$, shown in B is approximately 3.2.

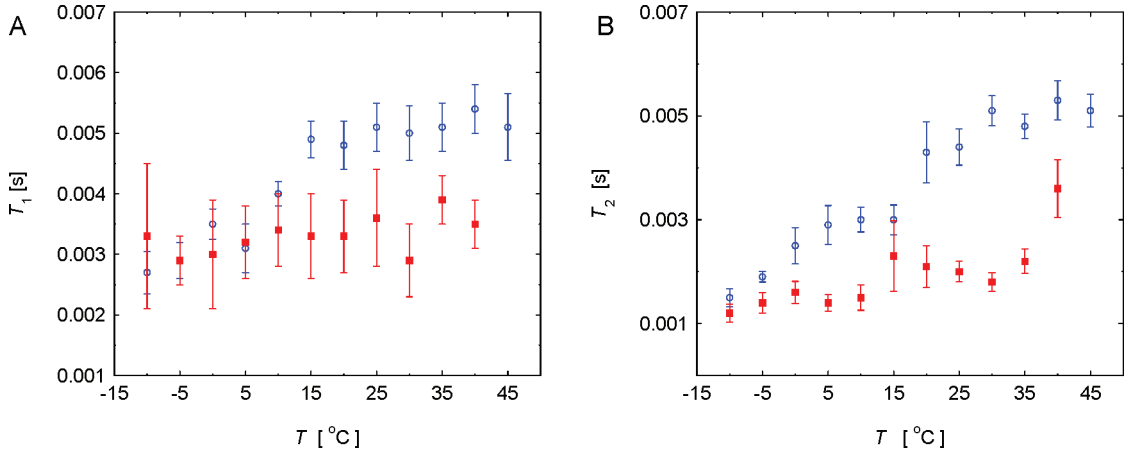

Figure 8. Experimental results of the ^2H (A) T_1 and (B) T_2 NMR relaxation times of the H_2O-hydrated $[VPG^*VG^*]_3$ peptide as a function of temperature. In the experiments, the temperature of the sample was first increased from −10 to 45 °C (blue, open circles) and then decreased back to −10 °C (red, filled squares). Each experimental data point took approximately 10 h to acquire. The time between the first and the last experiment was approximately 2 weeks. Estimation of the error bars is described in the text.

of temperature. The error bars shown in Figure 8 were estimated by considering the standard deviation of all measured T_1 and T_2 times in the 2D experiment. To be clear, we performed an exponential fit to the experimental data and used the derived standard deviation of the values determined from the exponential fits as estimates of the errors in the relaxation rates. We found that this method was similar to considering the width of the distributions in T_1 or T_2 dimensions in the 2D T_1-T_2 correlation maps.

In this temperature-dependent study, the sample temperature was first increased from −10 to 45 °C and then decreased back to −10 °C; the experiment at each temperature was performed for approximately 10 h with an average of 5 h of temperature equilibration between experiments; approximately 2 weeks time elapsed between the first and the last experiment. A difference in T_1 and T_2 relaxation times between the heating and the cooling cycles is revealed from Figure 8, indicating a thermal hysteresis of the Gly α-deuteron dynamics. In addition, a decrease in the slope of $T_1(T)$ and $T_2(T)$ heating curves is observed near 30 °C in Figure 8. To be clear, Figure 8A shows a plot of the T_1 and Figure 8B the T_2 versus temperature. In the heating curves (shown in blue circles) we observe a change in the slope of the relaxation times versus temperature near 30 °C; the slope appears to reduce. To give insight into the possible physical properties that may cause this reduction, we determined the number of water molecules within 0.35 nm of the Gly α-protons by MD simulation. Figure 9A highlights results from this computation: a reduction in the number of water molecules is observed near 30 °C. The reduction of localized water near the Gly α-protons in the simulation appears to be correlated to the observation of a change in the slope of the $T_1(T)$ and $T_2(T)$ heating curves revealed in the experimental data. The observed thermal hysteresis in the Gly α-deuteron dynamics may be due to structural changes that ensue from the inverse temperature transition even after the temperature is reduced.

According to the Bloembergen−Purcell−Pound (BPP) theory, the autocorrelation function of motion with a single correlation

dx.doi.org/10.1021/jp208966k |J. Phys. Chem. B 2012, 116, 555–564

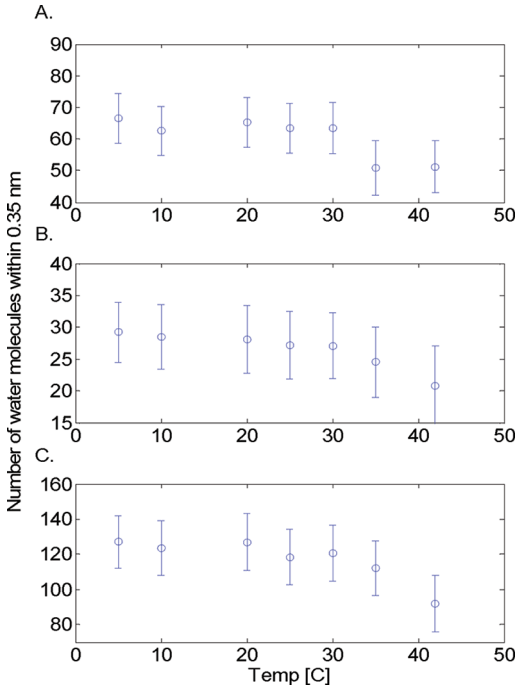

Figure 9. MD-derived simulation results highlighting the number of localized water molecules within 0.35 nm of (A) Gly α-protons, (B) Val α- and β-protons, and (C) Val γ-protons of the $[VPGVG]_3$ peptide. Error bars shown in the figure represent the statistical standard deviation over 1 ns of simulation time.

time is given by[50]

$$K(\tau) = \langle F(t)F^*(t)\rangle e^{-|\tau|/\tau_c} \quad (1)$$

where τ_c is the correlation time, $F(t)$ is a function of position of spatial coordinates, and the brackets, $\langle\rangle$, represent an average over all possible coordinates. The spectral density is the Fourier transform of eq 1 and given by

$$J(\omega) = \langle F(t)F^*(t)\rangle \frac{2\tau_c}{1 + (\omega\tau_c)^2} \quad (2)$$

where ω is the Larmor frequency. For ^{2}H nuclei, the NMR relaxation is governed by the quadrupolar interaction. The function $F(t)$ for the quadrupolar interaction is angular dependent, and the averaging process depends on the anisotropy of the motion of the nucleus. An important point that should be made clear is that the average $\langle F(t)F^*(t)\rangle$ is a constant that multiplies the spectral density. The spectral density functions for the T_1 and T_2 relaxation times are given by[51]

$$\frac{1}{T_1} = \frac{3}{40}C_q\left\{\frac{\tau_c}{1 + (\omega_D\tau_c)^2} + \frac{4\tau_c}{1 + 4(\omega_D\tau_c)^2}\right\} \quad (3)$$

$$\frac{1}{T_2} = \frac{1}{20}C_q\left\{9\tau_c + \frac{15\tau_c}{1 + (\omega_D\tau_c)^2} + \frac{6\tau_c}{1 + 4(\omega_D\tau_c)^2}\right\} \quad (4)$$

In eqs 3 and 4 C_q is the quadrupolar interaction strength and ω_D is the Larmor frequency for ^{2}H. For isotropic motion C_q is

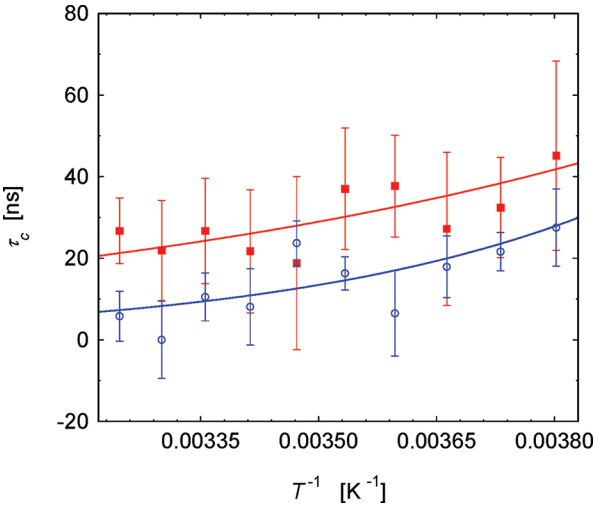

Figure 10. Measured correlation times (τ_c) of the Gly α-deuterons of the H_2O-hydrated $[VPG^*VG^*]_3$ peptide as a function of inverse temperature, T^{-1}. Blue open circles represent the experimental data when the sample temperature was increased; red filled squares indicate the data when the temperature was subsequently decreased. Solid lines are the best fits to $\tau_c = \tau_C^0 \exp(E_{act}/k_BT)$, where τ_C^0 is a constant, and the best-fit parameters for the activation energy are $E_{act} = (20.0 \pm 3.1)$ kJ/mol when heated and $E_{act} = (10.9 \pm 2.8)$ kJ/mol when cooled. For the blue open circles $\chi^2/\nu = 0.88$, and for the red filled squares $\chi^2/\nu = 0.23$, where χ^2/ν is the reduced chi square of the fit. Error bars shown were propagated from the error bars in the measured T_1 and T_2 relaxation times.

given by

$$C_q = 4\pi^2\left(1 + \frac{\eta^2}{3}\right)\left(\frac{e^2qQ}{h}\right)^2 \quad (5)$$

where η is the asymmetry parameter of the ^{2}H electric field gradient and $(e^2qQ)/h$ is the quadrupolar coupling constant. However, for anisotropic motion, C_q will be scaled by a constant. The motion of the nuclear spin in question at a particular site may be complex. In our analysis of the data we assumed a single correlation time to model the complex motion. Using eqs 3 and 4 the τ_c of the Gly α-deuterons was determined from the measured T_1 and T_2 values for all temperatures studied and are plotted in Figure 10. To be clear, eqs 3 and 4 are a system of two equations with two unknowns (τ_c and C_q) and determination of either parameter requires a measurement of both T_1 and T_2 relaxation times. With the sample temperature raised to 45 °C or cooled from 45 °C back to −10 °C, the correlation time appears to fit well within the experimental uncertainties to an Arrhenius law, from which we determined $E_{act} = (20.0 \pm 3.1)$ kJ/mol when heated and $E_{act} = (10.9 \pm 2.8)$ kJ/mol when cooled for the Gly α-deuterons. The reduction in the activation energy of the Gly α-deuterons also appears to be correlated to the extent of exposure to water resulting from the structural changes that ensue from the inverse temperature transition.

We also performed the 2D T_1-T_2 correlation experiments on the hydrated $[VPGV^*G]_3$ peptide; an example of the 2D T_1-T_2 map at 30 °C is shown in Figure 7B. Different from the 2D map of $[VPG^*VG^*]_3$ shown in Figure 7A, two distinguishable peaks are revealed in Figure 7B, indicating that there are two different

dx.doi.org/10.1021/jp208966k | J. Phys. Chem. B 2012, 116, 555–564

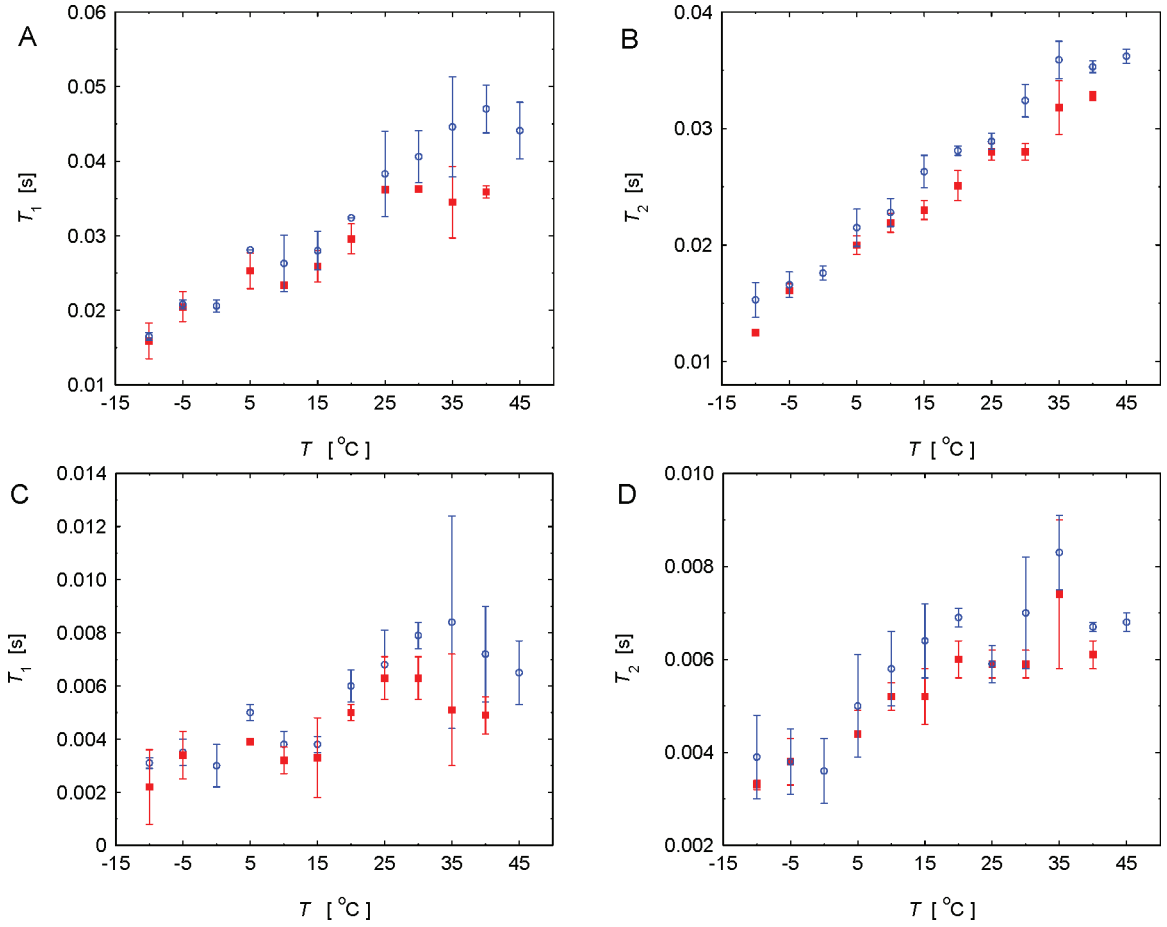

Figure 11. Experimental results of the ^{2}H (A) Val γ-T_1, (B) Val γ-T_2, (C) Val α- and β-T_1, and (D) Val α- and β-T_2 NMR relaxation times of the H_2O-hydrated $[VPGV^*G]_3$ peptide as a function of temperature. In the experiments, the temperature of the sample was first increased from −10 to 45 °C (blue open circles) and then decreased back to −10 °C (red filled squares). Each experimental data point took approximately 10 h to acquire, and the time between the first and the last experiment was approximately 2 weeks. Estimation of the error bars is described in the text.

relaxation times among all valine deuterons. The ratio of the signal intensities of the two peaks is measured to be approximately 6:2, and the larger intensity peak has larger T_1 and T_2 relaxation times corresponding to faster motion. The larger intensity peak is therefore attributed to the Val γ-deuterons (labeled Val_γ in Figure 7B) and the smaller intensity peak to the Val α- and β-deuterons (labeled $Val_{\alpha,\beta}$ in Figure 7B). Similar features shown in Figure 7B are observed for all temperatures studied. In addition to the expected difference in mobility of the Val α- and β-deuterons and Val γ-deuterons, the assignment of the two signals in the 2D T_1 and T_2 map was further confirmed by investigating the line widths, relative intensities, and chemical shifts of the ^{2}H spectra of the hydrated $[VPGV^*G]_3$ peptide. The measured T_1 and T_2 relaxation times associated with different deuterons are plotted in Figure 11 as a function of temperature. The error bars shown in the figure were estimated using a similar technique described previously for the Gly α-deuterons.

Referring to Figure 11, the thermal hysteresis in relaxation times is also observed for all Val deuterons of the hydrated $[VPGV^*G]_3$ peptide, but the effect appears to be smaller than that observed in the Gly α-deuterons shown in Figure 8. Referring to Figure 11, a change in the slopes of the $T_1(T)$ and $T_2(T)$ heating curves at approximately 30 °C is observed for all Val deuterons. To be clear, Figure 11 shows T_1 and T_2 versus temperature for all Val deuterons. The heating curves (shown as blue circles), in all cases, show a reduction in slope near 30 °C. Figure 9B and 9C highlights MD simulation results of the number of localized water molecules at the Val α- and β-protons and the Val γ-protons. The figures show a reduction in localized water near 30−35 °C at all sites, and the findings appear to be correlated to the experimental observation of a reduction in the slope of the $T_1(T)$ and $T_2(T)$ heating curves near this temperature.

The correlation times of Val γ-deuterons were determined using eqs 3 and 4 from the measured T_1 and T_2 values and are shown in Figure 12. Different from the correlation times of the Gly α-deuterons shown in Figure 10, there is no measurable difference in correlation times of Val γ-deuterons, within our experimental uncertainty, as the sample temperature is varied. For the lyophilized peptides one might expect that methyl correlation times would decrease with increasing temperature. For example, the jump rate of methyl groups in polycrystalline L-alanine were observed to approximately double with increasing temperature from −120 to −70 °C.[52] In the hydrated $[VPGVG]_3$ peptide, the inverse temperature transition drives an increase in side-chain contacts and an expulsion of localized water. While the increase in temperature may normally increase side-chain mobility, steric hindrance arising from the increase in side-chain contacts, the reduction in radius of gyration, and the reduction

dx.doi.org/10.1021/jp208966k | J. Phys. Chem. B 2012, 116, 555–564

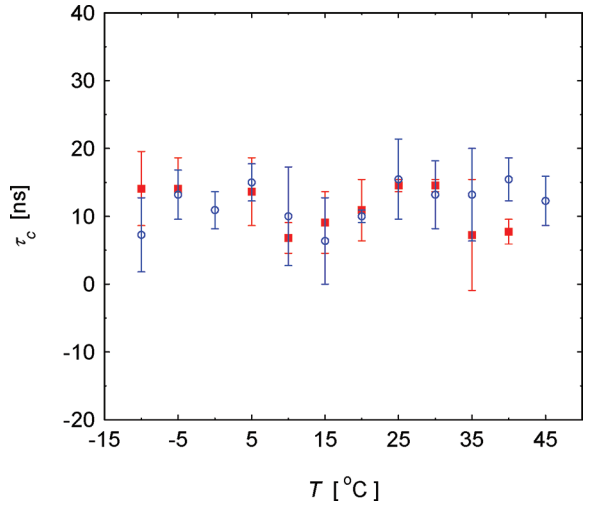

Figure 12. Measured correlation times, τ_c, of the Val γ-deuterons of the H_2O-hydrated $[VPGV^*G]_3$ peptide as a function of temperature (T). Blue open circles represent the experimental data when the sample temperature was increased; red filled squares indicate the data when the temperature was subsequently decreased. The error bars shown were propagated from the error bars in the measured T_1 and T_2 relaxation times.

in localized water would reduce side-chain motion. The competition of these mechanisms may be manifested in the temperature dependence of τ_c for the Val γ-deuterons shown in Figure 12. Lastly, it is worth noting that the correlation time determined from the T_1 and T_2 values using eqs 3 and 4 has a large uncertainty when T_1 and T_2 are approximately equal. The method used to determine τ_c therefore becomes challenging to implement for the measured Val α- and β-deuteron relaxation times shown in Figure 11C and 11D.

In addition to the observation of a thermal hysteresis reported here, the thermal hysteresis of the elastin-like peptides poly(VPGVG) and poly(VPAVG) has been experimentally observed by differential scanning calorimetry and turbidity (by monitoring the change in absorbance at 300 nm).[23] In their study, a clear hysteresis is evident in the calorimetry data over a time scale of approximately 10 min in the range from −5 to 60 °C as well as the turbidity over a range of approximately 7−40 °C. While these calorimetry and turbidity studies probe the macroscopic behavior of the polypeptides in solution, the methods implemented herein have provided for site-specific, microscopic information relating to the hysteresis that may be relevant in light of continued efforts to design artificial, biologically inspired elastomers.[53,54]

CONCLUSION

In this work we investigated the valine and glycine backbone and side-chain dynamics of the elastin mimetic peptide $[VPGVG]_3$ by ^2H quadrupolar echo spectroscopy and 2D T_1-T_2 correlation NMR. A key feature of the experimental data is the observation of a thermal hysteresis when the sample temperature is increased from −10 to 45 °C and subsequently cooled back to −10 °C. Using an Arrhenius model, the measured activation energies of the Gly α-deuterons are (20.0 ± 3.1) kJ/mol when the sample is heated and (10.9 ± 2.8) kJ/mol when cooled. The observed reduction in the activation energy of the Gly α-dueterons appears to be correlated to a well-known inverse temperature transition of the peptide; a process by which the peptide radius of gyration and number of localized water molecules and peptide−water hydrogen bonds reduce with increasing temperature from approximately 20 to 42 °C. In addition, the experimental data indicate that the measured correlation times of the Val γ-deuterons appear to be invariant with temperature. It is argued that the increase in the number of side-chain contacts and reduction of localized water counteract the thermally driven process that would otherwise increase the mobility of the Val γ-deuterons. Lastly, the experimentally measured $T_1(T)$ and $T_2(T)$ curves of all Val and Gly deuterons show a reduction in slope upon heating at approximately 30 °C that appears to be correlated to the extent of localized water as demonstrated by MD simulation.

AUTHOR INFORMATION

Corresponding Author

*Phone: +1 718 951 5000 ext 2873. Fax: +1 718 951 4407. E-mail: gboutis@brooklyn.cuny.edu.

ACKNOWLEDGMENT

We thank Yi-Qiao Song of Schlumberger-Doll Research for allowing us to implement the ILT algorithm and Laura J. Juszczak, Lesley Davenport, and Richard Magliozzo for useful discussions. G.S.B. acknowledges support from the Professional Staff Congress of the City University of New York and NIH grant no. 7SC1GM086268-03. The content is solely the responsibility of the authors and does not necessarily represent the official views of the National Institute of General Medical Sciences or the National Institutes of Health.

REFERENCES

(1) Urry, D. W. *J. Protein Chem.* **1988**, *7*, 1–34.
(2) Urry, D. W.; Parker, T. M. *J. Muscle Res. Cell Motil.* **2002**, *23*, 543–559.
(3) Debelle, L.; Tamburro, A. M. *Int. J. Biochem. Cell Biol.* **1999**, *31*, 261–272.
(4) Muiznieks, L. D.; Weiss, A. S.; Keeley, F. W. *Biochem. Cell Biol.* **2010**, *88*, 239–250.
(5) Partridge, S. M.; Davies, H. F.; Adair, G. S. *Biochem. J.* **1955**, *61*, 11–21.
(6) Lillie, M. A.; Gosline, J. M. *Int. J. Biol. Macromol.* **2002**, *30*, 119–127.
(7) Lillie, M. A.; Gosline, J. M. *Biopolymers* **1990**, *29*, 1147–1160.
(8) Mistrali, F.; Volpin, D.; Garibaldo, G. B.; Ciferri, A. *J. Phys. Chem.* **1971**, *76*, 142–150.
(9) Urry, D. W. *J. Protein Chem.* **1987**, *7*, 1–34.
(10) Urry, D. W.; Shaw, R. G.; Prasad, K. U. *Biophys. Res. Commun.* **1985**, *130*, 50–57.
(11) Urry, D. W.; Trapane, T. L.; Prasad, K. U. *Biopolymers* **1985**, *24*, 2345–2356.
(12) Urry, D. W.; Trapane, T. L.; Prasad, K. U. *Biochemistry.* **1985**, *24*, 5182–5189.
(13) Li, B.; Darwin, A. V.; Dagett, V. *J. Mol. Biol.* **2001**, *305*, 581–592.
(14) Mammi, M.; Gotte, L.; Pezzin, G. *Nature* **1968**, *225*, 371–373.
(15) Hoeve, C. A. J.; Flory, P. J. *Biopolymers* **1974**, *13*, 677–686.
(16) Weis-Fogh, T.; Anderson, S. O. *Nature* **1970**, *227*, 718–721.
(17) Gary, W. R.; Sandberg, L. B.; Foster, J. A. *Nature* **1973**, *246*, 21–28.
(18) Hong, M.; Isailovic, D.; McMillan, R. A.; Conticello, V. P. *Biopolymers* **2003**, *70*, 158–168.
(19) Yao, X. L.; Hong, M. *J. Am. Chem. Soc.* **2004**, *126*, 4199–4210.
(20) Yao, X. L.; Conticello, V. P.; Hong, M. *Magn. Reson. Chem.* **2004**, *42*, 267–275.
(21) Speiss, H. W. *Polym. Sci.* **1983**, *261*, 193–209.

(22) Peemoeller, H.; Shenoy, R. K.; Pintar., M. M. *J. Magn. Reson.* **1981**, *45*, 193–204.
(23) Reguera, J.; Lagaron, J. M.; Alonso, M.; Reboto, V.; Calvo, B.; Rodriguez-Cabello, J. C. *Macromolecules* **2003**, *36*, 8470–8476.
(24) Macho, V.; Brombacher, L.; Speiss, H. W. *Appl. Magn. Reson.* **2001**, *20*, 405–432.
(25) Vold, R. L.; Hoatson, G. L. *J. Magn. Reson.* **2009**, *198*, 57–72.
(26) Gall, C. M.; Diverdi, J. A.; Opella, D. J. *J. Am. Chem. Soc.* **1981**, *103*, 5039–5043.
(27) Shaefer, J.; Stejkal, E. O.; Mckary, R. A. *J. Magn. Reson.* **1984**, *57*, 85–92.
(28) Rice, D. M.; Wittebort, R. J.; Griffin, R. G.; Meirvitch, E.; Stimson, E. R.; Meinwald, Y.; Freed, J. H.; Sheraga, H. A. *J. Am. Chem. Soc.* **1981**, *103*, 7707–7710.
(29) Frey, M. H.; Opella, S. J.; Rockwell, A. L.; Gierasch, L. M. *J. Am. Chem. Soc.* **1985**, *107*, 1946–1951.
(30) Burke, P. A.; Griffin, R. G.; Klibanov, A. M. *Biotechnol. Bioeng.* **1993**, *42*, 87–94.
(31) Leo, G. C.; Colgano, L. A.; Valentine, K. G.; Opella, S. J. *Biochemistry* **1987**, *26*, 854–862.
(32) Vugmeyster, L.; Ostrovsky, D.; Ford, J. J.; Burton, S. D.; Lipton, A. S.; Hoatson, G. L.; Vold, R. L. *J. Am. Chem. Soc.* **2009**, *131*, 13651–13658.
(33) Struts, A. V.; Salgado, G. F. J.; Martinez-Mayorga, K.; Brown, M. F. *Nat. Struct. Mol. Biol.* **2011**, *18*, 392–394.
(34) Song, Y.-Q.; Venkataramanan, L.; Hurlimann, M. D.; Flaum, M.; Frulla, P.; Straley, C. *J. Magn. Reson.* **2002**, *154*, 261–268.
(35) Englis, A. E.; Whittall, K. P.; Joy, M. L. G.; Henkelman, R. M. *Magn. Reson. Medicine.* **1991**, *22*, 425–434.
(36) Wong, P. Z. *Methods in the Physics of Porous Media*; Academic Press: San Diego, 1999.
(37) Halperin, W. P.; DŠOrazio, F.; Bhattacharja, S.; Tarczon, J. C. In *Molecular Dynamics in Restricted Geometries*; Klafter, J., Drake, J. M., Eds.; Wiley: New York, 1989; Chapter 11.
(38) Kleinberg, R. L.; Farooqui, S. A.; Horsfield, M. A. *J. Colloid Interface Sci.* **1993**, *158*, 195–198.
(39) Hills, B.; Costa, A.; Marighet, N.; Wright, K. *Appl. Magn. Reson.* **2005**, *28*, 13–27.
(40) McDonald, P. J.; Korb, J.-P.; Mitchell, J.; Monteilhet, L. *Phys. Rev. E* **2005**, *72*, 011409-1–011409-9.
(41) Sun, C.; Boutis, G. S. *New J. Phys.* **2011**, *13*, 025026-1–025026-16.
(42) Furo, I.; Hedin, N. *J. Magn. Reson.* **2001**, *152*, 214–216.
(43) Jorgensen, W. L.; Tirado-Rives, J. *J. Am. Chem. Soc.* **1988**, *110*, 1657–1666.
(44) Berendsen, H. J. C.; Postma, J. P. M.; DiNola, A.; Haak, J. R. *J. Chem. Phys.* **1984**, *81*, 3684–3690.
(45) Hess, B.; Kutnzer, C.; Spoel, D. V. D.; Lindahl, E. *J. Chem. Theory Comput.* **2008**, *4*, 435–477.
(46) Teleman, O.; Jonsson, B.; Engstrom, S. *Mol. Phys.* **1987**, *60*, 193–203.
(47) Schreiner, E.; Nicolini, C.; Ludolph, B.; Ravindra, R.; Otte, N.; Kohlmeyer, A.; Rousseau, R.; Winter, R.; Marx., D. *Phys. Rev. Lett.* **2004**, *92*, 148101–148105.
(48) Perry, A.; Stypa, M. P.; Tenn, B. K.; Kumashiro, K. K. *Biophys. J.* **2002**, *82*, 1086–1095.
(49) Ohgo, K.; Niemczura, W. P.; Ashida, J.; Okonogi, M.; Asakura, T.; Kumashiro, K. K. *Biomacromolecules* **2006**, *7*, 3306–3310.
(50) Bloembergen, N.; Purcell, E. M.; Pound, R. V. *Phys. Rev.* **1948**, *73*, 679–712.
(51) Abragam, A. *Principles of Nuclear Magnetism*; Oxford University Press: New York, 1961.
(52) Beshah, K.; Olejniczak, E. T.; Griffin, R. G. *J. Chem. Phys.* **1987**, *86*, 4730–4736.
(53) Pepe, A.; Armenante, A. M.; Bochicchio, B.; Tamburro, A. M. *Soft Matter* **2009**, *5*, 104–113.
(54) Lim, D. W.; Nettles, D. L.; Setton, L. A.; Chilkoti, A. *Biomacromolecules* **2008**, *9*, 222–230.